Journal of Colloid and Interface Science 626 (2022) 251–264

Contents lists available at ScienceDirect

Journal of Colloid and Interface Science

journal homepage: www.elsevier.com/locate/jcis

Mucus-penetrating nanoparticles based on chitosan grafted with various non-ionic polymers: Synthesis, structural characterisation and diffusion studies

Twana Mohammed M. Ways [a,h], Sergey K. Filippov [b,h], Samarendra Maji [c,d], Mathias Glassner [c], Michal Cegłowski [c,e], Richard Hoogenboom [c], Stephen King [f], Wing Man Lau [g], Vitaliy V. Khutoryanskiy [h,*]

[a] Department of Pharmaceutics, College of Pharmacy, University of Sulaimani, Sulaimani, 46001 Kurdistan Region, Iraq
[b] Pharmaceutical Sciences Laboratory, Faculty of Science and Engineering, Åbo Akademi University, Turku 20520, Finland
[c] Supramolecular Chemistry Group, Centre of Macromolecular Chemistry (CMaC), Department of Organic and Macromolecular Chemistry, Ghent University, Krijgslaan, 281 S4, B-9000 Ghent, Belgium
[d] Department of Chemistry, SRM Institute of Science and Technology, Kattankulathur, 603203 Kanchipuram, Tamil Nadu, India
[e] Adam Mickiewicz University in Poznan, Faculty of Chemistry, Uniwersytetu Poznańskiego 8, 61-614 Poznań, Poland
[f] ISIS Pulsed Neutron & Muon Source, Science and Technology Facilities Council, Rutherford Appleton Laboratory, Harwell Campus, Didcot OX11 0QX, UK
[g] School of Pharmacy, Faculty of Medical Sciences, Newcastle University, Newcastle upon Tyne NE1 7RU, UK
[h] Reading School of Pharmacy, University of Reading, Whiteknights, Reading RG6 6AD, UK

GRAPHICAL ABSTRACT

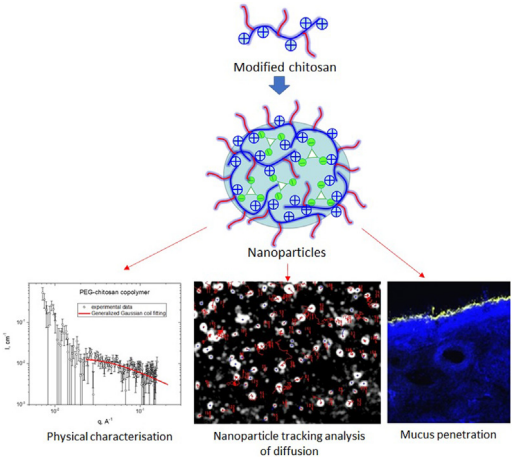

ARTICLE INFO

Article history:
Received 15 March 2022
Revised 13 June 2022
Accepted 24 June 2022
Available online 27 June 2022

Keywords:
Chitosan

ABSTRACT

Transmucosal administration offers numerous advantages for drug delivery as it usually helps to avoid first pass metabolism, provides rapid onset of action, and is a non-invasive route. Mucosal surfaces are covered by a viscoelastic mucus gel layer which acts as a protective barrier preventing the entrance of harmful substances into the human tissues. This function of mucus also inhibits the diffusion of drugs and nano-formulations and can result in a significant reduction of their efficacy. The design of mucus-penetrating nanoparticles can overcome the barrier function of mucus which may lead to better therapeutic outcomes. In this study, chitosan was chemically modified by grafting short chains of poly(ethylene glycol), poly(2-hydroxyethyl acrylate), poly(2-ethyl-2-oxazoline), or poly(*N*-vinyl pyrrolidone) and

* Corresponding author.
E-mail address: v.khutoryanskiy@reading.ac.uk (V.V. Khutoryanskiy).

https://doi.org/10.1016/j.jcis.2022.06.126

Nanoparticles
Mucus penetration
Diffusion
Drug delivery

the resulting chitosan derivatives were used to prepare nanoparticles using an ionic gelation method with sodium tripolyphosphate. These nanoparticles were characterised using dynamic light scattering, transmission electron microscopy, small-angle neutron scattering and nanoparticle tracking analysis. Small-angle neutron scattering data revealed the presence of a large amount of water inside these nanoparticles and lack of a heterogeneous internal structure. The nanogel model with low crosslinking density is suggested as the most feasible model to describe the structure of these nanoparticles. The studies of the behaviour of these nanoparticles in bovine submaxillary mucin solutions and their penetration into sheep nasal mucosa indicated greater diffusivity of modified chitosan nanoparticles compared to unmodified chitosan nanoparticles with the best results achieved for the chitosan grafted with poly(*N*-vinyl pyrrolidone).

1. Introduction

Transmucosal drug delivery encompasses all routes of administration when dosage forms are directly interacting with mucosal membranes of the human body and the drug molecules are supposed to diffuse through the mucosal lining before reaching epithelial cells. The established routes of transmucosal administration include oromucosal (buccal, sublingual, and gingival), ocular, nasal, oesophageal gastrointestinal, vaginal, rectal and intravesical [1-8]. Administration of drugs via mucosal routes is advantageous as it helps to avoid first pass metabolism, provides rapid onset of action and is non-invasive. In some cases, administration via mucosal routes could achieve targeted delivery of drugs to particular organs. For example, application of eye drops allows targeting of ocular tissues [3] and nasal administration provides direct access to the brain [9].

It is known that a mucosal layer is continuously renewed in a process called mucus turnover, and the turnover rate varies depending on the physiological features of a particular organ. For example, rat intestinal mucus is renewed every 47–270 min [10]. The rapid movement of cilia propels the nasal respiratory mucus (known as mucociliary clearance) from the interior toward the posterior part of the nasal cavity resulting in a short mucus turnover time (15–20 min in human) [11]. In rats, the mucus turnover time of nasal respiratory mucosa is about 10 min [12].

Mucus often acts as a barrier for diffusion of nanomedicines and even small drug molecules [13,14]. Different therapeutic areas can potentially benefit from the development of nanomaterials with enhanced diffusivity through mucus. This will be beneficial for the delivery of small drug molecules, vaccines and biopharmaceutical agents to prevent, manage or treat respiratory diseases including viral infections, chronic rhinitis, asthma, chronic obstructive pulmonary disease and cystic fibrosis, which are often characterised by excessive mucus production [15-18]. Inefficient diffusion of nanomaterials through viscous vaginal fluids also limits some therapies for sexually transmitted infections [19]. Mucus-penetrating medicines could also benefit therapies of some gastrointestinal conditions, for example, infections caused by *Helicobacter pylori* bacteria residing in the mucosal lining of the stomach and duodenum, responsible for the majority of ulcers in the stomach and small intestine as well as for some cancers [20]. Facilitated diffusion of nanoparticles in different viscous body fluids is also of interest for other non-mucosal therapeutic areas, e.g. intraocular drug delivery [21,22].

Traditionally, it is believed that formulations adhering to mucosal linings could be used for more efficient transmucosal drug delivery. However, more recently Hanes et al. [23,24] demonstrated that PEGylation of 200 nm polystyrene nanoparticles makes them less adhesive and facilitates their penetration through mucus gels. These pioneering studies have triggered further research into the development of various mucus-penetrating PEGylated delivery systems [25-28].

Alternatives to PEGylation are currently also of great interest in the development of mucus-penetrating systems [29]. Recently, we demonstrated that thiolated silica nanoparticles functionalised with poly(2-methyl-2-oxazoline) and poly(2-ethyl-2-oxazoline) had a greater diffusivity in porcine gastric mucin dispersions and porcine gastric mucosa compared to their thiolated parent nanomaterial [30,31]. However, these silica nanoparticles, similarly to the polystyrene nanoparticles used by Hanes et al. [23,24] can only be used as a model system to study diffusion, not as a drug vehicle because of their non-porous nature.

In this study, we evaluated the potential of several non-ionic hydrophilic polymers in the design of mucus-penetrating nanoparticles based on chitosan. Four different water-soluble polymers - poly(ethylene glycol) (PEG), poly(2-hydroxyethyl acrylate) (PHEA), poly(2-ethyl-2-oxazoline) (POZ) and poly(*N*-vinyl pyrrolidone) (PVP) - were grafted onto chitosan (hereinafter referred as PEG-, PHEA-, POZ- and PVP-chitosan, respectively). These polymers were chosen due to their non-ionic nature that was expected to make nanoparticles with mucus-inert surfaces and stealth properties. The structures of chitosan modified with these polymers are shown in Figs. S1, S2, S4 and S6 in the Supplementary Information. These modified polysaccharide macromolecules were used to prepare nanoparticles through complex formation with sodium tripolyphosphate (hereinafter referred to as PEG-, PHEA-, POZ- and PVP-chitosan nanoparticles, respectively). The structure of the nanoparticles formed by unmodified and modified chitosan was characterised using dynamic light scattering, transmission electron microscopy and small-angle neutron scattering. The diffusivity of these nanoparticles in mucin solutions and through sheep nasal mucosa was studied. To the best of our knowledge, this is the first study that provides a comparison of mucus-penetrating particles decorated with four polymers of different nature and it is the first report of using PVP and PHEA as polymers to facilitate mucus penetration.

2. Materials and methods

2.1. Materials

Medium molecular weight chitosan (degree of deacetylation 75–85%), trifluoroacetic acid (TFA), D_2O, 1-ethyl-3-(3-dimethylaminopropyl)-carbodiimide hydrochloride (EDAC), *N*-hydroxysuccinimide (NHS), mucin from bovine submaxillary glands Type I-S (BSM), sodium tripolyphosphate (TPP), 4′,6-diamidino-2-phenylindole dihydrochloride (DAPI), and D-(+) glucosamine hydrochloride were purchased from Sigma-Aldrich (Gillingham, UK). Uranyl acetate dihydrate was purchased from Agar Scientific (UK). Sodium acetate trihydrate, Molecular Probes™ Alexa Fluor™ 546 NHS ester (Alexa Fluor™ 546), glacial acetic acid, dimethyl sulfoxide (DMSO), sodium hydroxide (NaOH) and CellPath™ OCT embedding matrix (OCT) were purchased from Fisher Scientific (UK). Dialysis membrane with a molecular cut-off of

12–14 kDa was purchased from Medicell International Ltd., UK. Phosphotungstic acid hydrate was purchased from Fluka. Hydroxyethyl acrylate (HEA, 96%, Aldrich) was destabilized by passing the monomer through a basic aluminium oxide column prior to polymerization. *N*-vinylpyrrolidone (NVP, 99%, Acros) was purified by vacuum distillation. 2,2′-azobis(isobutyronitrile) (AIBN), potassium ethyl xanthogenate and 2-bromopropionic acid 99% were obtained from Sigma-Aldrich. AIBN was purified by recrystallization twice in methanol before use. HPLC grade solvents *N,N*-dimethylacetamide (DMA), diethyl ether and dichloromethane were obtained from Sigma-Aldrich, *N,N*-dimethylformamide (DMF) was obtained from Biosolve and *n*-hexane from Fischer Scientific. 2-(butylthiocarbonothioylthio)propanoic acid (BTTCP) was synthesised as described by Ferguson et al. [32]. Xanthate CTA (2-((ethoxycarbonothioyl)thio)propanoic acid) (ECTTPA) was synthesised by a general procedure described previously by Pound et al. [33]. Acetonitrile (Aldrich) was dried in a solvent purification system (J. C. Meyer). 2-Ethyl-2-oxazoline (EtOx; Aldrich), methyl 2-bromoacetate and piperidine were distilled over barium oxide and stored under argon. All other chemicals were of analytical grade, purchased from Sigma-Aldrich or Acros Organics and were used as received.

2.2. Methods

2.2.1. Synthesis of PHEA-COOH, POZ-COOH and PVP-COOH

The details of the synthesis of PHEA-COOH, POZ-COOH and PVP-COOH are provided in the Supplementary Information.

2.2.2. Synthesis of PEG-, PHEA-, POZ- and PVP-chitosan

Four modified chitosan (PEG-, PHEA-, POZ- and PVP-chitosan) were synthesised as follows. To 80 mg medium molecular weight chitosan, 11.5 mL acetic acid (1% v/v) was added. The mixture was continuously stirred for 20 h at room temperature. The pH of the chitosan solutions was increased to 6 using 5 M NaOH solution. PEG-COOH (117 mg), PHEA-COOH (117 mg dissolved in 5 mL deionised water) and POZ-COOH (117 mg) and PVP-COOH (100 mg) was added to the chitosan solutions. Then after 5 min stirring, NHS (13.5 mg) was added to each and stirred for 30 min. EDAC (22.4 mg) was then added and stirred for 24 h. The products were dialysed against deionised water (4 L, 8 total changes, 12–14 kDa MWCO dialysis membrane) at room temperature for at least 3 days. The products were recovered by lyophilisation using a Heto Power Dry LL 3000 freeze-drier (Thermo Electron Corporation). The % of yield was calculated according to equation (1).

$$\text{Yield } \% = \frac{W_1}{W_2 + W_3} \times 100 \quad (1)$$

W1 is the weight of the freeze-dried modified chitosan. W2 and W3 are the weights of the unmodified chitosan and carboxyl-terminated non-ionic polymers (PEG-, PHEA-, POZ- and PVP-COOH) in the reaction mixture, respectively.

The percentage of grafting by weight (GW %) was calculated according to the method reported by Bhattarai et al. [34] as follows:

$$GW\% = \frac{W_g - W_n}{W_g} \times 100 \quad (2)$$

where W_g is the weight of the freeze-dried grafted polymer and W_n is the weight of native chitosan in the reaction mixture.

2.2.3. NMR spectroscopy

^{1}H NMR spectra were recorded using a Bruker Nanobay 400 MHz NMR spectrometer. 1 mL D_2O was placed in a vial. Then to this, 10 μL of TFA was added. The polymers were added to the acidified D_2O (except for PEG-chitosan where only D_2O was used as a solvent) and stirred for 16 h at room temperature. The degree of acetylation (DA) of the unmodified chitosan was calculated as follows [35]:

$$DA = \frac{ICH_3/3}{IH_2 - H_6/6} \times 100 \quad (3)$$

where I CH_3 is the integral intensity of *N*-acetylated protons and I H_2-H_6 is the sum of the integral intensity of protons number 2, 3, 4, 5 and 6.

The degree of substitution (DS) of the modified chitosan was calculated using ^{1}H NMR spectroscopy by integrating related peaks of the grafted polymers against specific chitosan peak in the modified chitosan. The related peaks were marked in the Supplementary Information (Fig. S1, 2, 4 and 6).

2.2.4. FTIR spectroscopy

FTIR spectra of the freeze-dried polymers were recorded using a NICOLET iS5 FTIR spectrophotometer (ThermoScientific, UK). The spectra were collected from an average of 16 scans, with a resolution of 4 cm^{-1} over the range of 4000–400 cm^{-1}.

2.2.5. pH-solubility profile

Solubility of the modified and unmodified chitosan was measured at different pH at room temperature using a turbidimetric technique. The polymers were dissolved (0.5 mg/mL, 20 mL) in 1% v/v acetic acid and left stirring for 24 h. The turbidity (absorbance) of the solutions was measured at room temperature using a BioTek Epoch plate reader at 400 nm using 1% v/v acetic acid as a blank. 200 μL aliquots were used. The pH was adjusted by the addition of either 1 M NaOH solution or 1% v/v acetic acid. The results are reported as the average of the turbidity of 3 samples at each pH point ± standard deviation.

2.2.6. Labelling unmodified and modified chitosan with Alexa Fluor™ 546

Unmodified and modified chitosan were dissolved in 9.66 mL 1% v/v acetic acid to form 5 mg/mL, solutions. The pH was increased to 6 using 5 M NaOH solution. Alexa Fluor™ 546 was dissolved in DMSO (5 mg/mL), then 138 μL Alexa Fluor™ 546 solution (equivalent to 0.69 mg Alexa Fluor™ 546) was added to the chitosan solution and the reaction mixture was stirred for 4 h at room temperature in the dark. Then the product was dialysed against deionised water in the dark using 12–14 kDa MWCO dialysis membrane (for 96 h, 1 L for 5 changes). To determine the Alexa Fluor™ 546 content, chitosan solutions (0.2 mg/mL in 1% v/v acetic acid) were prepared by stirring overnight in the dark. Then the solutions were diluted according to the calibration curve with ultrapure water in the dark. The pH was adjusted to 6 using 0.5 M NaOH solution. The fluorescence intensity of three separate samples was measured using a fluorescence spectrometer (Cary Eclipse, Varian Inc., US). In order to establish a calibration curve, serial dilutions of Alexa Fluor™ 546 in ultrapure water (50, 25, 12.5, 6.25 and 3.125 ng/mL) were prepared by diluting Alexa Fluor™ 546 stock solution (5 mg/mL in DMSO). Finally, Alexa Fluor™ 546 content was calculated with reference to the calibration curve.

2.2.7. Preparation of nanoparticles

Unmodified chitosan and modified chitosan nanoparticles were prepared using an ionic gelation method according to Calvo et al. [36] but with some modifications. After optimisation trials, the following protocol was selected. Polymer solutions (1 mg/mL in 1% v/v acetic acid) were prepared and the pH was increased to 5.5 using 5 M NaOH. 1 mg/mL TPP solution was prepared by dissolving the calculated amount of TPP in deionised water. Before mixing, both

TPP and chitosan solutions (pH 5.5) were filtered through a 0.2 μm syringe filter. Then, 4 mL TPP solution was added dropwise to the polymer solutions (8 mL) over a period of 5 min. The suspensions were stirred for another 30 min at room temperature. Alexa Fluor™ 546- labelled chitosan and PEG-chitosan nanoparticles were prepared similarly to unlabelled chitosan nanoparticles. However, for Alexa Fluor™ 546-labelled PHEA-, POZ- and PVP-chitosan nanoparticles, 2 mL TPP solution was added to 4 mL Alexa Fluor™ 546-labelled chitosan solutions with the rest performed exactly as described for the unlabelled chitosan nanoparticles. In case of Alexa Fluor™ 546-labelled nanoparticles, the experiments were conducted in the dark.

2.2.8. Characterisation of the nanoparticles

2.2.8.1. Dynamic light scattering (DLS). The size and ξ-potential of the nanoparticles were measured using a Zetasizer Nano-ZS (Model: ZEN3600, Malvern, UK). For the size measurements, the samples were diluted (1:100 for unlabelled nanoparticles and 1:20 for Alexa Fluor™ 546-labelled nanoparticles) with ultrapure water before analysis. A refractive index of 1.59 and an absorbance of 0.01 were used for all measurements. Viscosity (0.8872 cP) and refractive index (1.33) of water were used as dispersant parameters. The samples were equilibrated for 60 s and the measurements were conducted in triplicate for 10 s per run, with 12 runs per reading at 25 °C. The measurement angle was set to 173° backscatter. For the data processing, the normal resolution analysis model (general purpose algorithm) was selected. ξ-potential values were measured using DTS-1070 folded capillary tube cuvettes (Malvern, UK). Samples were diluted with ultrapure water (1:10) before analysis. Samples were measured using 3 repeats of 20 sub-runs per reading. The information on nanoparticle sizes was evaluated by taking both Z averaged and number-weighted value of hydrodynamic diameter (D_h). Z averaged D_h is predominantly sensitive to the largest particles available in solution whereas number-weighted value represents the smallest, most populated fraction of the nanoparticles. We used number-weighted value for the comparison with the TEM data. Polydispersity index (PDI) was taken as an estimate of sample polydispersity. PDI value was calculated as the ratio of the second k_2 and first cumulants k_1, PDI = 2 k_2/k_1^2, where cumulants k_1 and k_2 are coefficients in the first and second coefficients in the Taylor series expansion of a correlation function $g_1(t)$; $\ln[g_1(t)]=- k_1\tau + k_2 \tau^2/2$. To obtain the ξ-potential, data was processed using auto mode analysis model. At least 3 samples were measured and processed using the Smoluchowski model (Fκa = 1.50) to convert electrophoretic mobility data to ξ-potential.

2.2.8.2. Nanoparticle tracking analysis (NTA). The nanoparticles were also characterised by NTA using the NanoSight instrument (LM10 system, LM14 laser module, top plate and green 532 nm laser, Malvern, UK). For the NTA measurements, Alexa Fluor™ 546-labelled nanoparticles suspensions were diluted (1:10,000) with ultrapure water (pH 5.5, acidified with 1% v/v acetic acid). Fluorescence mode was used for the NTA measurement of the nanoparticles. 1 mL of diluted sample was taken using a 1 mL syringe and the syringe loaded onto the NTA syringe pump. A sCMOS camera and the NTA 3.2 software were used to capture and process the motion of the nanoparticles. The camera level was set to 16 and the detection thresholds were 5. A syringe pump speed of 50 AU was selected to minimise the fluorescence bleaching of the nanoparticles. The viscosity of water was used as the diluent viscosity. Automatic maximum jump mode, blur and minimum track length were used for all NTA measurements. The temperature was fixed at 25 °C. For each sample, 6 videos of 60 s were recorded and for each nanoparticle type, three separate samples were analysed. Finally, the mean and the mode of size and the mean diffusion coefficient were reported. 100 nm non-fluorescent polystyrene latex (diluted 1:150,000 with ultrapure water) was used as a standard, however, the scatter mode was used to measure the size of these standard nanoparticles. NTA method has a lower limit of detection in the range of 20–50 nm and depends on nanoparticle density and refractive index. For chitosan-based nanoparticles we expect the NTA low limit to be 50 nm.

2.2.8.3. Transmission electron microscopy (TEM). TEM was conducted using a JEM-2100 PLUS Electron Microscope (JEOL, USA) at an accelerating voltage of 200 kV. One drop of nanoparticle suspension was placed on a piece of parafilm. A carbon-coated copper grid was dipped into a drop of nanoparticle suspension and left for 1 min. The excess nanoparticle suspension was then removed by a filter paper. Then a drop of 2% w/v phosphotungstic acid solution was placed on the parafilm. The grid was immersed in the stain solution for 30 s and then the excess stain was also removed by a filter paper. The samples were then air dried and submitted to the instrument. At least 3 images were taken and the size of the nanoparticles was measured using the ImageJ software (National Institutes of Health, USA).

2.2.8.4. Small-angle neutron scattering (SANS). SANS experiments were performed on the LOQ time-of-flight diffractometer at the ISIS Pulsed Neutron Source (Rutherford Appleton Laboratory, UK). A simultaneous *q*-range (=$4\pi \sin\theta / \lambda$, where 2θ is the scattering angle) of 0.007–0.24 $Å^{-1}$ was achieved by utilizing an incident wavelength range of 2.2–10.0 Å at 25 Hz with a sample-detector distance of 4.15 m. The beam diameter at the samples was collimated to 12 mm diameter. Each scattering data set was corrected for the detector efficiency and spatial linearity, the measured neutron transmission and background scattering, and converted to scattering cross-section data (hereafter referred to as intensity, I) using the Mantid framework (version 3.12.1) [37]. These corrected data were then placed on an absolute scale (cm^{-1}) using the scattering from a partially-deuterated polystyrene blend of known molecular weight measured with the same instrument configuration [38].

Prior to the SANS experiments, several attempts were made to purify the nanoparticles and disperse them in D_2O (to minimise the incoherent background from hydrogen atoms in the samples and improve the signal-to-noise). Preliminary experiments showed that dialysis against 1 L of deionised water resulted in aggregation of unmodified chitosan nanoparticles. Thus, in this study, dialysis against D_2O to replace H_2O was not used. Also, replacing any H_2O with D_2O, and 1% v/v acetic acid with 1% v/v TFA in the formulations for the preparation of both unmodified and PEG-chitosan nanoparticles failed to produce nanoparticles (aggregates were observed with unmodified chitosan whereas a clear solution was obtained with PEG-chitosan and thus no DLS measurement could be performed). In this attempt, 1 mg/mL TPP solution was added to 1 mg/mL unmodified chitosan or modified chitosan solutions (1:2) to prepare unmodified chitosan and modified chitosan nanoparticles, respectively. Then, centrifugation was used to replace some of the H_2O with D_2O. The particles were centrifuged using an Amicon Ultra™ centrifugal filter unit (0.5 mL capacity, 3 kDa MWCO, Millipore (UK) Limited) at the speed of 10,000 rpm (Sanyo, Micro Centaur, UK) for 30 min. Then, 200 μL D_2O was added to the nanoparticles retentate and centrifuged at 10,000 rpm for a further 15 min. Finally, another 200 μL D_2O was added to the nanoparticles retentate and the particle size was measured using DLS (after dilution with ultrapure water, 1:10). The particle dispersions were placed in sealed vials, wrapped with parafilm and stored in a refrigerator (4 °C) until the day of the SANS experiments. Centrifuged unlabelled chitosan nanoparticles (in D_2O) were loaded into circular 1 mm path length quartz cells (Hellma UK, Type 120 or Starna Scientific, Type 32) and another

cell was filled with D_2O as a background. Non-centrifuged unlabelled and Alexa Fluor™ 546-labelled unmodified chitosan, PEG-, POZ- and PVP-chitosan nanoparticles (in H_2O) were also loaded into similar 1 mm path length cells. For these samples a solution consisting of [4 mL 1% v/v acetic acid (pH 5.5 by 5 M NaOH) + 2 mL 1 mg/mL TPP in H_2O solution] was used as a background.

Additionally, chitosan, PEG-, POZ- and PVP-chitosan solutions (1 mg/mL in 1% v/v TFA in D_2O) were filtered through 0.45 μm syringe filter. These solutions were loaded into 5 mm path length quartz cells of the same type. This time 1% v/v TFA in D_2O was used as a background. The cells were mounted on an enclosed temperature-controlled sample changer. All SANS experiments were performed at 25 °C.

The scattering from PEG-, PHEA-, POZ- and PVP-chitosan graft copolymers was fitted using SASFit software 0.94.11 to the form factor of a Generalized Gaussian coil (P_1) [39].

$$P_1(q,Rg,\nu) = I_0 \frac{U^{\frac{1}{2\nu}}\Gamma\left(\frac{1}{2\nu}\right) - \Gamma\left(\frac{1}{\nu}\right) - U^{\frac{1}{2\nu}}\Gamma\left(\frac{1}{2\nu},U\right) + \Gamma\left(\frac{1}{\nu},U\right)}{\nu U^{1/\nu}} + \ bgd \tag{4}$$

where $U=(2\nu+1)(2\nu+2)q^2R_G^2/6$, I_0 is the scattered intensity at $q = 0$, R_G is the gyration radius, ν is the Flory exponent, and Γ is the incomplete Gamma function.

The scattering from unlabelled and fluorescently labelled nanoparticles was either fitted to:

(i) a model of polydisperse homogeneous spheres (P_2) with a fixed Schulz-Zimm polydispersity $\sigma/<R>=0.2$

$$P_2(q,R) = \Delta\rho^2 V^2 \left(\frac{(\sin(qR) - qR\cos(qR))}{(qR)^3}\right)^2 + bgd \tag{5}$$

where $\Delta\rho$ is the scattering length density difference between the nanoparticles and the bulk medium, V is the sphere volume, and R is the hard sphere radius, or;

(ii) monodisperse homogeneous ellipsoids (P_3) with eccentricity $\varepsilon = 2$

$$P_3(q,R) = \Delta\rho^2 \left(\frac{4\pi\varepsilon R^3}{3}\right)^2 \int_0^{\pi} \left(\frac{(\sin(qR) - qR\cos(qR))}{(qR)^3}\right)^2 \sin\theta d\theta + bgd \tag{6}$$

where R is now the equatorial semi-axis, εR is the semi-principal axis of ellipsoid, and θ is the angle between the axis of the ellipsoid and the vector **q**.

Whilst the background scattering from D_2O subtracted nicely from the scattering data, the buffer scattering was slightly under subtracted (Fig. S13-S20). However, this was compensated for by fitting the residual background level, *bgd*.

2.2.9. Fluorescence spectroscopy

Fluorescence emission spectra of Alexa Fluor™ 546-labelled chitosan nanoparticles and 0.5% w/v BSM solution were obtained between 560 and 750 nm at an excitation wavelength of 554 nm using a fluorescence spectrometer (Cary Eclipse, Varian Inc., US). For the measurements, the nanoparticles were diluted (1:50) with ultrapure water, whereas the mucin solution was measured without dilution. The experiments were conducted in triplicate.

2.2.10. Viscosity measurement of BSM solution

0.5% w/v BSM solutions (3 × 25 mL) were prepared by dissolving the required amount of BSM in ultrapure water. The samples were stirred overnight at room temperature. After complete hydration, the pH of the solutions was decreased to 5.5 using 1% v/v acetic acid. Rheological analysis was performed using an AR 2000ex rheometer (TA Instruments, UK) with a 40 mm parallel plate. First, 0.5 mL sample was measured to find the linear viscoelastic region of BSM. This measurement was conducted at 25 °C with a solvent trap in place. First, at a constant frequency of 1 Hz, a strain sweep was performed between 0.01 and 10%. Then, at a constant strain of 4% a frequency sweep between 0.01 and 10 Hz was performed. Thus it was found that a frequency of 1 Hz and strain of 4% was optimum for providing the linear viscoelastic region. Temperature ramp experiments (at 1 °C/minute, between 20 and 40 °C) were then performed at frequency of 1 Hz and strain of 4%. Values of the viscosity were plotted as a function of temperature and the viscosity of the mucin solution at 25 °C was calculated using the trendline equation. This viscosity was later used in the NTA diffusion study of the nanoparticles in BSM solution.

2.2.11. Evaluation of diffusion of chitosan nanoparticles in BSM solutions

NTA was used to evaluate the diffusion of chitosan nanoparticles in BSM solution. Initially, 4 different concentrations of BSM solution (0.1, 0.25, 0.5 and 1% w/v) were evaluated for their background fluorescence noise and their consistency. Next, Alexa Fluor™ 546-labelled chitosan nanoparticles were first diluted in ultrapure water (pH 5.5, 1:100). Then the diluted particles were mixed with 0.5% w/v BSM solution (pH 5.5, 1:100). Then, 1 mL of the mixture was injected into the NTA system and the flow rate was set at 50 AU. The diffusion of the nanoparticles in the mucin solutions was visualised at 25 °C. The videos were recorded through a 565 nm cut-off filter. Each individual mucin solution was mixed 3 times with each of the nanoparticle types and thus generated 9 × 6 × 60 s videos (n = 9). The measured viscosity of 0.5% w/v BSM solution (3.05 cP, found from the rheological analysis) was used for processing the diffusion data. The other parameters were set as described for size measurements of the nanoparticles using NTA in section 2.2.8.2.

2.2.12. Penetration of chitosan nanoparticles into sheep nasal mucosa

The penetration of chitosan nanoparticles was studied using whole thickness sheep nasal mucosa. The tissues were used immediately following animal slaughter and delivery from a local abattoir (P.C. Turner Abattoirs, Farnborough, UK). The nasal septum mucosa was segmented into 1 × 1.5 cm^2 and placed in a plastic Petri dish and transferred to a temperature-controlled incubator (32 °C). 20 μL Alexa Fluor™ 546-labelled chitosan nanoparticles were added onto the nasal mucosal tissues and incubated at 32 °C for 5, 15 and 30 min without any washing. After each time point, tissues were transferred and covered with OCT matrix and placed on dry ice for overnight storage. The frozen tissue blocks were then stored in sealed bags in the freezer at −80 °C until processing.

To prepare tissue slices, the tissues were cross-sectioned using a Bright 5040 cryostat (Bright Instrument Co. Ltd., UK) which was loaded with an MB35 Premier Disposable Microtome blade (34° cutting angle, length × width × thickness: 80 × 8 × 0.25 mm, Thermo Scientific, UK). The blade angle and thickness was set to 2.5° and 20 μm, respectively. The specimen and chamber temperature were −20 and −25 °C, respectively. The slices were cut upward through the mucosal layer and transferred to SuperFrost Plus™ Adhesion slides (Thermo Scientific, UK) and air dried for 30 min before storage. At least 10 slices were prepared for each time point. Sheep nasal mucosa without any exposed nanoparticles was used as a background control.

The fluorescence microscopy was performed using a Leica MZ10F fluorescence stereomicroscope (Leica Microsystems, UK). The images were taken at exposure time 344 ms, gain 3X, gamma

1, pseudocolour 565 nm, maximum intensity, magnification of 3.2 and ET CY3 filter. At least 10 images were recorded for each time point.

The images were analysed using ImageJ software (National Institutes of Health, USA) and the depth of penetration was measured according to Mansfield et al. [31] with some modifications. The images were opened using the software and the scale was set. A line was drawn along the mucosal layer and the fluorescence intensity profile of the line was plotted. The plot showed the fluorescence peak width, which indicates the depth of penetration of the nanoparticles into the nasal mucosa. This graphical profile was converted into numbers using the list option. The depth of penetration was calculated by subtracting the value of the start point from the value of the end point of the peak. For each image, this procedure was repeated 5 times at random regions of mucosal barrier and thus for each sample at each time point, 50 profiles were generated.

Additionally, to investigate how far the nanoparticles penetrated into the nasal mucosa, 75 μL DAPI solution (1.5 μg/mL in deionised water) was added to stain the cross sections and incubated overnight in the dark at room temperature. At least 6 slices were stained. Fluorescence microscopy was performed the following day in a dark using Zeiss Axio Imager.A1 upright epifluorescent microscope with AxioVision Rel. 4.8 software. At least 3 images for each time point were taken. Each image was taken first with Alexa 546 (yellow) and then with DAPI (blue) filters. The images were then merged and exported as composite images using AxioVision Rel. 4.8 software.

2.2.13. Statistical analysis

Unless otherwise stated, all measurements were conducted in triplicate and the data are expressed as mean ± standard deviation (SD). The data were analysed using the SPSS Statistics 21 program (IBM, US). The statistical significance of any difference between groups was determined using one-way analysis of variance (ANOVA) with the least significant difference (LSD) post-hoc test. Independent sample t-tests were performed to compare each pair of data sets. Differences were considered statistically significant at $p < 0.05$.

3. Results and discussion

3.1. Characterisation of unmodified and modified chitosan

Chitosan is a cationic mucoadhesive polysaccharide having free amino and hydroxyl groups. The presence of these groups in chitosan allows possible chemical modifications [40]. We hypothesised that modification of chitosan into a more hydrophilic derivative might impart stealth properties to the modified chitosan which eventually could be used in the formulation of mucus penetrating nanoparticles. In this study, four chitosan derivatives have been synthesised by reacting chitosan with four water-soluble polymers (carboxyl terminated-PEG, PHEA, POZ and PVP) using EDAC/NHS chemistry. The synthetic procedure provided high yields (Table 1). The DS of unmodified and modified chitosan was determined using ^{1}H NMR spectroscopy (Fig. S1 and Table 1).

As shown in Fig.S1 the ^{1}H NMR spectrum of the unmodified chitosan shows the peaks at 3.06, 3.57–3.80 and 1.97 ppm corresponding to H2, H3-6 and $NHCOCH_3$, respectively. H1 was not observed and this is consistent with the literature claiming that H1 can only be determined at temperatures higher than 25 °C [41]. The ^{1}H NMR spectrum of PEG-chitosan showed a peak at 3.35 ppm corresponding to OCH_3 group of PEG-COOH and the peaks related to H3, H4, H5 and H6 overlapped with the peaks of OCH_2CH_2 and OCH_2 groups (b, c and d) (3.35–3.89 ppm) (Fig. S1).

Table 1
Characterisation of the synthesised modified chitosan, including isolated yield, grafting by weight (GW) and degree of substitution (DS).

Types of materials	Yield (%)	GW (%)	DS (%)
PEG-chitosan	77	47	16
PHEA-chitosan	63	36	6
POZ-chitosan	65	38	16
PVP-chitosan	80	44	- [a]

[a] It was impossible to determine the degree of substitution due to overlap of ^{1}H NMR signals.

The peaks of PEG-COOH and PEG-chitosan were identified and compared as highlighted in the literature [42]. The DS (DPEG %) was calculated according to the following equation:

$$\mathrm{DPEG}\% = \frac{\mathrm{I(OCH3)/3}}{\mathrm{I(H2)}} \times 100 \quad (7)$$

The ^{1}H NMR spectrum of PHEA-chitosan showed additional peaks related to PHEA (most notably the peak at 4.10 ppm (b) (Fig. S2). The ^{1}H NMR spectrum of PHEA-COOH is also shown in Fig. S3 The DS (DPHEA%) was calculated using the following equation:

$$\mathrm{DPHEA}\% = \frac{\frac{\mathrm{I(b)PHEA}}{2\times43}}{\mathrm{I(H2)}} \times 100 \quad (8)$$

The ^{1}H NMR spectrum of POZ-chitosan showed 2 new characteristic peaks related to POZ at 0.96 ppm (CH_3 of side chain, i.e. 3H) and 2.27 ppm (CH_2 of side chain, i.e. 2H and N-CH_2 of the end group). The 4 protons of the CH_2 groups of the main chain overlapped with H2-H6 peaks of chitosan (Fig. S4). The ^{1}H NMR spectrum of POZ-COOH is also shown in Fig. S5. The DS (DPOZ %) was calculated using the following equation:

$$\mathrm{DPOZ}\% = \frac{\frac{\mathrm{ICH3\ POZ}}{3\times50}}{\mathrm{I(CH3)/3}} \times 100 \quad (9)$$

The ^{1}H NMR spectrum of the PVP-chitosan also showed peaks related to PVP. Unfortunately, the DS of PVP-chitosan could not be determined using ^{1}H NMR spectroscopy as the peaks of PVP and chitosan overlapped (Fig. S6). The ^{1}H NMR spectrum of PVP-COOH is shown in Fig. S7.

The FTIR spectra of the unmodified and modified chitosan are shown in Fig. S8. The FTIR spectrum of unmodified chitosan showed broad bands at 3000–3600 cm^{-1} due to stretching vibration of O—H and N—H bonds and 1649 cm^{-1} due to amide group (*N*-C=O) stretching. For PEG-chitosan, the characteristic peaks from the PEG backbone at 842, 961 and 2882 cm^{-1} were observed. The peak at 1654 cm^{-1} was ascribed to amide groups in the linker between PEG and chitosan. A very weak ester peak at 1746 cm^{-1} was also observed [43]. The FTIR spectrum of PHEA-chitosan showed a characteristic carbonyl peak (C=O stretching) at 1724 cm^{-1}, the aliphatic C—H stretching peak at 2929 cm^{-1}, CH_2 stretching at 1447 cm^{-1} and O—H stretching at 3357 cm^{-1}. POZ-chitosan showed peaks related to POZ at 1633 cm^{-1} (C=O stretching), 1471 cm^{-1} (C—H deformation), 1423 cm^{-1} (CH_3 symmetrical deformation/CH_2 bending) and 1239 cm^{-1} (C—N stretch). The FTIR spectrum of PVP-chitosan showed peaks at 3370 cm^{-1} (O—H stretching), 2921 cm^{-1} (symmetric stretching CH_2 ring), 1654 cm^{-1} (C=O stretching), 1288 cm^{-1} (CH_2 wag), 1152 cm^{-1} (C—N stretch), 845 cm^{-1} (C—C ring) and 642 cm^{-1} (*N*-C=O bend). As such, both ^{1}H NMR and FTIR spectroscopy confirmed successful grafting of the non-ionic polymers to chitosan.

The main problem with chitosan is its poor aqueous solubility, especially when the pH is higher than its pK_a (pK_a is ~ 6.5, depending on factors such as DA and the molecular weight) [44]. Turbidimetry was used to determine the pH-solubility profiles of

unmodified and modified chitosan. Fig. 1 shows that unmodified chitosan was soluble (illustrated by low turbidity or absorbance) over acidic pH ranges. However, it underwent rapid aggregation (indicated by high turbidity or absorbance) at pH $\geq$ 7.38. This result was expected, because at acidic pH, the amino groups of chitosan undergo protonation, whereas at near neutral pH, they become deprotonated [45]. All the modified chitosans, however, showed full aqueous solubility (illustrated by low turbidity) at the studied pH ranges (3–10). This result is due to the grafting of the polymers to the chitosan macromolecules which reduces the intra- and inter-molecular hydrogen bonding and enhances the hydrophilicity of the conjugates [46].

3.2. Preparation and characterisation of unmodified and modified chitosan nanoparticles

The improved water-solubility of the modified chitosan is a highly important step toward the preparation of modified chitosan nanoparticles as dissolution of chitosan is necessary prior to ionic gelation. Chitosan nanoparticles can be prepared via electrostatic attractive interactions between positively charged chitosan and negatively charged TPP (Fig. 2). Although several studies have reported the formation of chitosan nanoparticles using TPP, the variation in the source of chitosan, which in turn leads to variation in the molecular weight, the DA, the viscosity and other properties, requires a full optimisation study to prepare chitosan nanoparticles from the unmodified chitosan and grafted chitosan derivatives. Some studies reported that there is no clear correlation between the mass ratio of chitosan/TPP and the size of the resulting chitosan nanoparticles [47]. Thus, several attempts have been reported to prepare nanoparticles aiming to have the smallest size with acceptable polydispersity index (PDI) (Table S1). PDI is the dimensionless measure of the broadness of the size distribution calculated from the cumulants analysis. The values of PDI range from 0 to 1 and the values > 0.7 indicate the size distribution is polydisperse and the samples may not be suitable for the DLS measurement (Table S1). The PDI value in the range of 0.2–0.5 stands for moderate polydispersity. The small particles with the low PDI can be prepared by changing the concentration of chitosan solution, weight ratio of chitosan/TPP, concentration of acetic acid, temperature of crosslinking and the pH of the chitosan and TPP solutions. CS16 (Table S1) was selected as the optimum formulation of unmodified chitosan nanoparticles. The same formulation was used to prepare modified chitosan nanoparticles. The DLS data showed that unlabelled unmodified and modified chitosan nanoparticles Z averaged value of D_h of 130–152 nm with a PDI of 0.24–0.29 indicating moderate polydispersity (Table 2). However, number-weighted values are in the range of 30–40 nm (Table 2, Fig. 2A). Such a difference is not surprising due to the moderate polydispersity of nanoparticles. The ξ-potential of each of the unlabelled modified chitosan nanoparticles was lower than the unmodified chitosan nanoparticles (Table 2). This may be attributed to the decrease in the number of protonated amino groups upon modification or the presence of a polymeric shell in modified chitosan nanoparticles which can mask the positive charges of chitosan.

Fig. 3 shows TEM images of the chitosan nanoparticles. The diameter of all unmodified and modified chitosan nanoparticles measured by TEM was in agreement with the number-weighted diameter measured by DLS (Table 2). TEM and number-weighed DLS data both confirm that the vast majority of nanoparticles have the size of 30–50 nm that co-exist with small fraction of larger particles having the size of 50–200 nm.

SANS experiments were conducted to characterise unlabelled and fluorescently labelled chitosan nanoparticles. Although the accumulation time was more than two hours per curve, all data have a rather low signal-to-noise ratio (Fig. S9-S20). The scattering from the PEG-, PHEA-, POZ- and PVP-chitosan copolymers was the weakest and show a typical behaviour for coil conformation (Fig. S9-S12). The radius of gyration (R_g) of the graft copolymers was in the range of 2–3 nm, which is consistent with average molecular weights of these polymers. The Flory exponent was varying in the range of 0.5–0.9. However, these values of the Flory exponent were subject to significant uncertainties that makes their use as a means of comparing the conformations of the graft copolymers useless. The scattering intensity for all unlabelled and fluorescently labelled chitosan nanoparticles is higher than the values observed for individual polymers, indicating the formation of larger objects in solution. Nevertheless, the data are again noisy, and we attribute this both to a high fraction of solvent inside the nanoparticles and low polymer concentration (1 mg/mL) leading to the very low scattering contrast reported from the fitting procedure (Table 3). A similar finding was recently observed for interpolyelectrolyte complexes [48]. Using a linearly-weighted relationship between scattering length densities of the unhydrated polymers and D_2O, allowed us to estimate the amount of solvent inside these nanoparticles (Table 3). Visual inspection of the scattering curves revealed no obvious features pointing to internal heterogeneity e.g. core–shell structure. Therefore, we fitted all the SANS data from the nanoparticles to two of the simplest homogeneous particulate form-factors: polydisperse spheres with fixed Schulz-Zimm polydispersity $\sigma/\langle R\rangle$ = 0.2 and monodisperse ellipsoids with eccentricity ε = 2. The values of polydispersity and eccentricity were assessed from the TEM images and kept fixed during the fitting procedure. As can be seen from Fig. S13-S20 and Table 3 both models work well and provide similar χ^2 values.

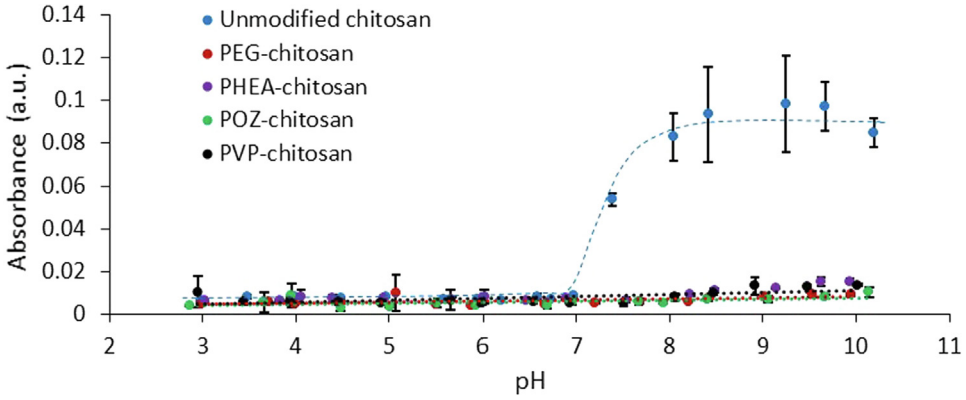

Fig. 1. pH-solubility profiles of unmodified and modified chitosan (mean ± SD, n = 3).

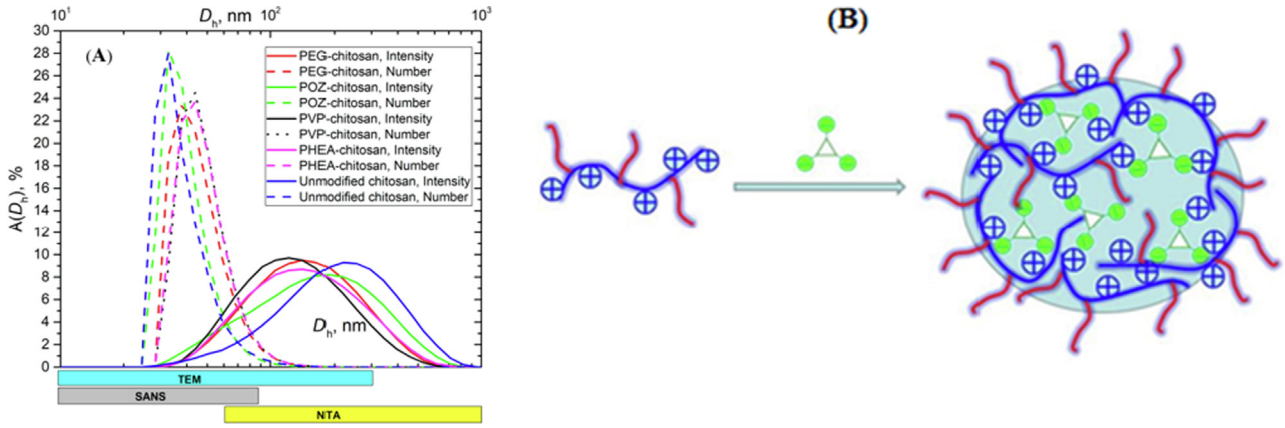

Fig. 2. (A) DLS intensity and number-weighted hydrodynamic diameter distribution for different unlabelled chitosan nanoparticles. (B) Diagram showing formation of nanoparticles between modified chitosan (positively charged structure) and TPP (negatively charged structure).

Table 2
Physicochemical properties of unlabelled chitosan nanoparticles (mean ± SD, n = 3).

Types of nanoparticles	Z-average diameter (nm)	Number-weighted D_h (nm)	PDI	ξ-potential (mV)	TEM diameter (nm)[a]
Unmodified chitosan	152 ± 13	37 ± 7	0.24 ± 0.02	25.5 ± 1.3	43 ± 15
PEG-chitosan	137 ± 23	35 ± 6	0.25 ± 0.03	13.4 ± 0.1	55 ± 15
PHEA-chitosan	142 ± 11	40 ± 3	0.29 ± 0.04	13.7 ± 0.1	41 ± 9
POZ-chitosan	145 ± 21	32 ± 13	0.28 ± 0.02	15.0 ± 0.3	31 ± 9
PVP-chitosan	130 ± 19	40 ± 5	0.28 ± 0.04	12.3 ± 1.6	33 ± 10

[a] For diameter measurements by TEM, 20 values from 20 individual nanoparticles from 3 different TEM images were used. Note: only individual particles were measured and fused particles were excluded.

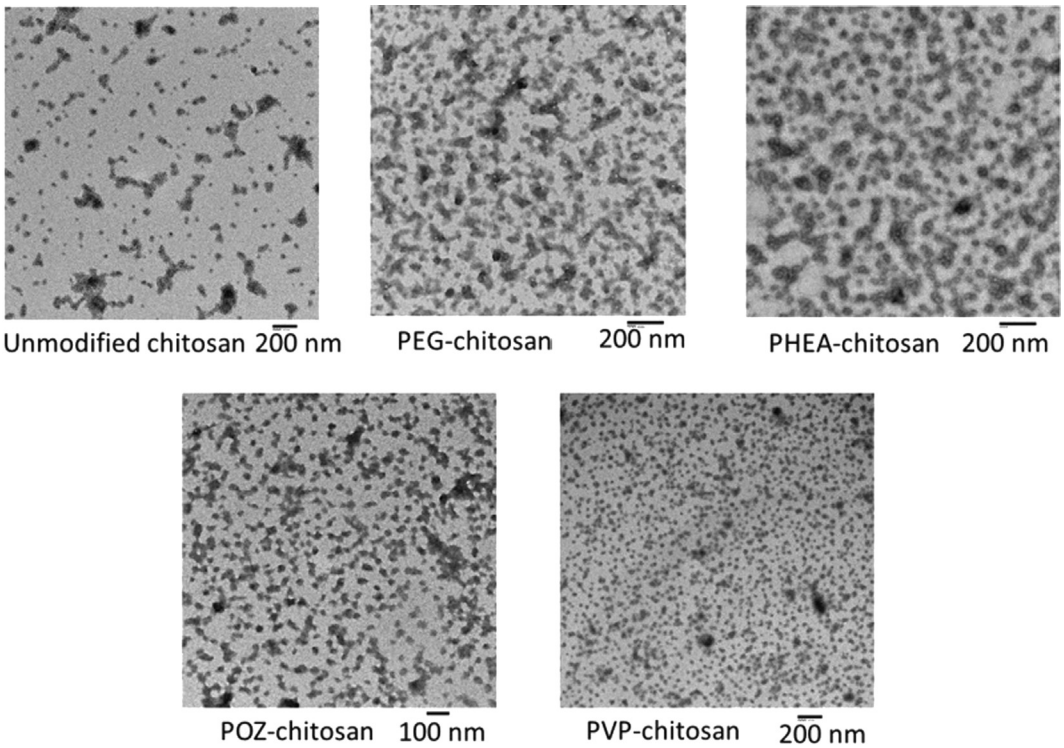

Fig. 3. TEM images of unmodified and modified chitosan nanoparticles.

There is a good agreement between the diameters from SANS and number-weighed values from DLS (Tables 2 and 3). The analysis of the SANS data suggests a highly hydrated nanogel structure for nanoparticles in solution.

To prepare fluorescent chitosan nanoparticles, unmodified and modified chitosan were first fluorescently labelled using Alexa Fluor™ 546 (Fig. S21A). The fluorescence labelling is essential for the diffusion study in BSM solutions and following penetration

Table 3
Physicochemical properties of unlabelled and fluorescently labelled chitosan nanoparticles from SANS fitting.

Types of nanoparticles		Ellipsoidal, ε = 2, D (nm)	χ2	Polydisperse spheres, σ = 0.2, D (nm)	χ2	Δρ, (10^8 cm^{-2})	x_{solv}, %
Unlabelled	Chitosan	17.6 ± 0.1	148	17.6 ± 0.2	149	18 ± 1	96
	PEG-chitosan	30.8 ± 0.2	166	31.8 ± 0.2	166	3 ± 1	99
	POZ-chitosan	25.6 ± 0.1	136	25.4 ± 0.3	135	6 ± 1	99
	PVP-chitosan	36.4 ± 0.3	192	35.0 ± 0.4	190	3.0 ± 0.3	99
labelled	Chitosan	21.8 ± 0.4	154	23.2 ± 0.2	153	10 ± 1	97
	PEG-chitosan	38.0 ± 0.3	130	39.4 ± 0.1	130	2.6 ± 0.4	99
	POZ-chitosan	39.2 ± 0.1	201	39.8 ± 0.1	200	2.1 ± 0.3	99
	PVP-chitosan	42.2 ± 0.1	133	42.2 ± 0.3	133	2.3 ± 0.3	99
	PHEA-chitosan	47.0 ± 0.1	99	47.6 ± 0.1	98	1.8 ± 0.2	99

through nasal mucosa. Analysis of the dialysis media showed that there was no free Alexa Fluor™ 546 in the labelled polymers (Fig. S22). The calibration curve which was used to calculate the Alexa Fluor™ 546 content of chitosan is shown in Fig. S23. Unmodified and modified chitosan showed similar Alexa Fluor™ 546 content (Table 4). However, the fluorescence intensity of the Alexa Fluor™ 546-labelled unmodified chitosan nanoparticles was lower than for modified chitosan nanoparticles (Fig. S21B and Table 4), which could be due to the stronger interaction between the amino groups of the unmodified chitosan and TPP, compared to the interaction between modified chitosan and TPP, resulting in a partial fluorescence quenching. In the case of modified chitosan, this interaction could be decreased as a significant number of amino groups have been substituted with the grafted chains of non-ionic polymers resulting in better hydration of nanoparticles and their greater fluorescence intensity compared to unmodified chitosan nanoparticles (Table 4).

It was possible to measure the diameter of the Alexa Fluor™ 546-labelled chitosan nanoparticles using DLS. This was because the excitation wavelength (absorption maxima, 554 nm) of Alexa Fluor™ 546-labelled chitosan nanoparticles is significantly lower than the wavelength of the laser used by the Zetasizer (633 nm, red laser) and thus no interference in light scattering was expected. This hypothesis is also supported by Geißler et al. [49] who showed that fluorescent-labelling does not have a significant impact on the size data of the polymeric nanoparticles using DLS and small-angle X-ray scattering especially when absorption maxima of the nanoparticles are different from the illuminating wavelength and the degree of fluorescent-labelling is not extremely high. Nevertheless, our data showed that the Alexa Fluor™ 546-labelled chitosan nanoparticles have a lower PDI than the unlabelled nanoparticles (Tables 2 and 4).

NTA can be used to measure the size, the concentration (particles/mL) and also the diffusion coefficient of the nanoparticles dispersed in liquid media [50]. Compared to DLS, it is a complimentary technique for the measurement of the size of the nanoparticles in the range of 50–500 nm [51,52] since it provides number-weighted size data. However, it is unable to detect particles smaller than 50 nm. Moreover, for polydisperse systems with moderate polydispersity, small particles scatter much less light and their probability to be detected is lower in comparison with larger particles. The NTA analysis of size was in agreement with the Z averaged DLS data (Table 4). The particle size distribution measured by NTA (Fig. 4) indicated that the prepared unmodified and modified chitosan nanoparticles have some fraction of 100–140 nm particles. The number-weighted data obtained from DLS also indicate the dominant fraction of 40–70 nm particles that are also visible with SANS method (Table 3).

3.3. Chitosan nanoparticles diffusion in BSM solution and penetration into sheep nasal mucosa

NTA is also a powerful technique for measuring the mean diffusion coefficient of nanoparticles in polymer solutions [53] and mucin dispersions [31]. To conduct diffusion studies, NTA should be performed in fluorescence mode instead of light scattering mode, enabling the visualisation of only the fluorescent nanoparticles. BSM solution (2% w/v, in pH 5 phosphate buffer solution) has been previously used to study mucoadhesive properties of polymeric microparticles [54]. 0.5% w/v BSM solutions were used in this study to reduce interference resulting from mucin autofluorescence. It is worthy to mention that the concentration of mucin solution in this study is lower than the mucin concentration in the nasal mucus (2% w/v) [55], but it is significantly higher than the concentration (0.1% w/v and even 0.001% w/v) used in some studies involving polymer- and nanoparticle-mucin interactions [56-58]. The viscosity of 0.5% w/v BSM solution at 25 °C was 3.05 ± 0.37 cP as determined by rheological analysis (Fig. S24).

NTA analysis revealed that the modified chitosan nanoparticles diffuse significantly faster in BSM solution ($p < 0.001$) compared to the unmodified chitosan nanoparticles (Fig. 5). The enhanced diffusivity of the modified chitosan nanoparticles can be due to the presence of non-ionic PEG, PHEA, POZ or PVP surface coating as shown in Fig. 2B. Lai et al. [24] showed that PEG coating of polystyrene nanoparticles facilitated their penetration in fresh undiluted human cervicovaginal mucus. We also previously demonstrated that PEGylation and POZylation of thiolated silica nanoparticles enhanced their diffusivity in porcine gastric mucin

Table 4
Characterisation of Alexa Fluor™ 546 labelled polymers and nanoparticles (mean ± SD, n = 3).

Materials	Alexa Fluor™ 546 content		Z-average diameter (nm, DLS)	Number-weighted D_h (nm)	Modal size (nm, NTA)	PDI (DLS)	ξ-potential (mV)	Diffusion coefficient in H_2O ($\times 10^4$ nm^2/s)	Maximal fluorescence intensity (a.u.)
	μmole/g of polymer	W% of polymer							
Unmodified chitosan	9.32 ± 0.02	1.080 ± 0.002	144 ± 1	40 ± 3	140 ± 10	0.17 ± 0.01	18 ± 2	310 ± 20	539 ± 1
PEG-chitosan	8.72 ± 0.05	1.01 ± 0.01	107 ± 1	59 ± 3	110 ± 10	0.10 ± 0.01	11.9 ± 0.5	440 ± 30	760 ± 10
PHEA-chitosan	10.10 ± 0.03	1.171 ± 0.003	134 ± 3	75 ± 6	128 ± 4	0.07 ± 0.02	11.8 ± 0.2	370 ± 10	760 ± 3
POZ-chitosan	9.60 ± 0.05	1.11 ± 0.01	119 ± 2	51 ± 2	110 ± 10	0.09 ± 0.02	12.5 ± 0.2	410 ± 10	743 ± 3
PVP-chitosan	8.89 ± 0.07	1.03 ± 0.01	112 ± 1	40 ± 3	110 ± 10	0.106 ± 0.003	12.0 ± 0.5	390 ± 10	677 ± 4

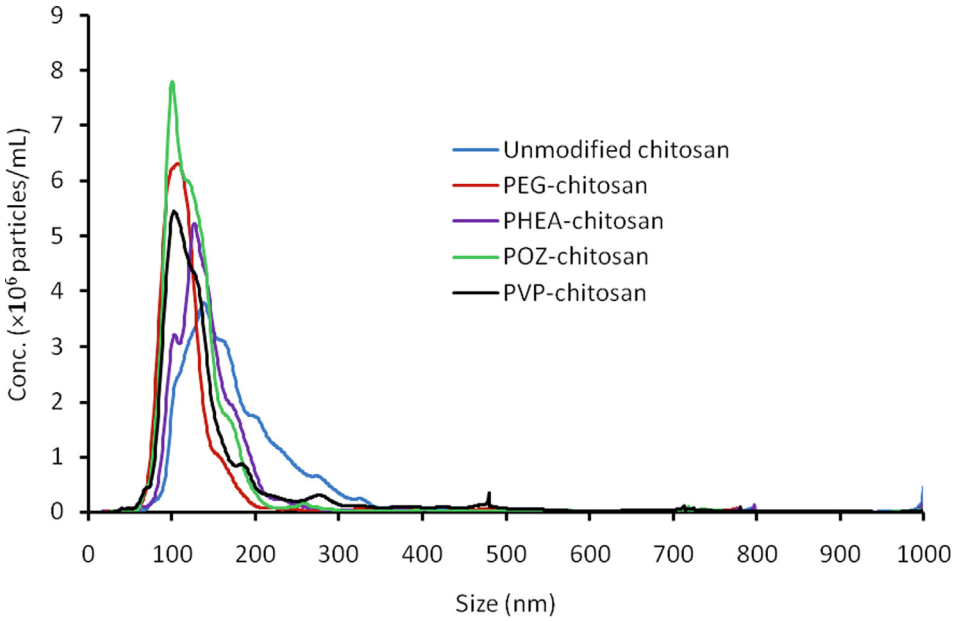

Fig. 4. Size distribution of Alexa Fluor™ 546-labelled unmodified and modified chitosan nanoparticles measured by NTA (mean, n = 3).

dispersion and through porcine gastric mucosa [31] and also reduced their mucoadhesiveness with regard to rat intestinal mucosa [59]. Casettari et al. [43] showed that PEGylated chitosan does not significantly enhance the permeability of fluorescein isothiocyanate-dextran macromolecules across a Calu-3 cell monolayer at pH 7.4, whereas they observed a dramatic permeability enhancement when the polymer was tested at pH 6. We conducted our diffusion study at pH 5.5 as preliminary experiments showed that unmodified chitosan nanoparticles undergo aggregation once diluted with ultrapure water (without any pH adjustment) for the NTA measurements. Other authors [43] did not report any possible reasons for the difference in the permeability at these two different pH values. However, they claimed that the enhancement could be due to the higher equivalent concentration of chitosan in PEGylated chitosan compared to unmodified chitosan and also the enhanced diffusivity of the PEGylated chitosan compared to unmodified chitosan [43]. The latter reason was also indirectly supported by Prego et al. [60], who observed that calcitonin loaded PEGylated chitosan nanocapsules with 1% PEGylation had a significantly less hypocalcaemic effect than nanocapsules with 0.5% PEGylation when orally administered to rats. They postulated that an increase in the degree of PEGylation might result in a decrease in the mucoadhesive properties of chitosan. Thus, a weak interaction between PEGylated chitosan nanocapsules (with 1% PEGyla-

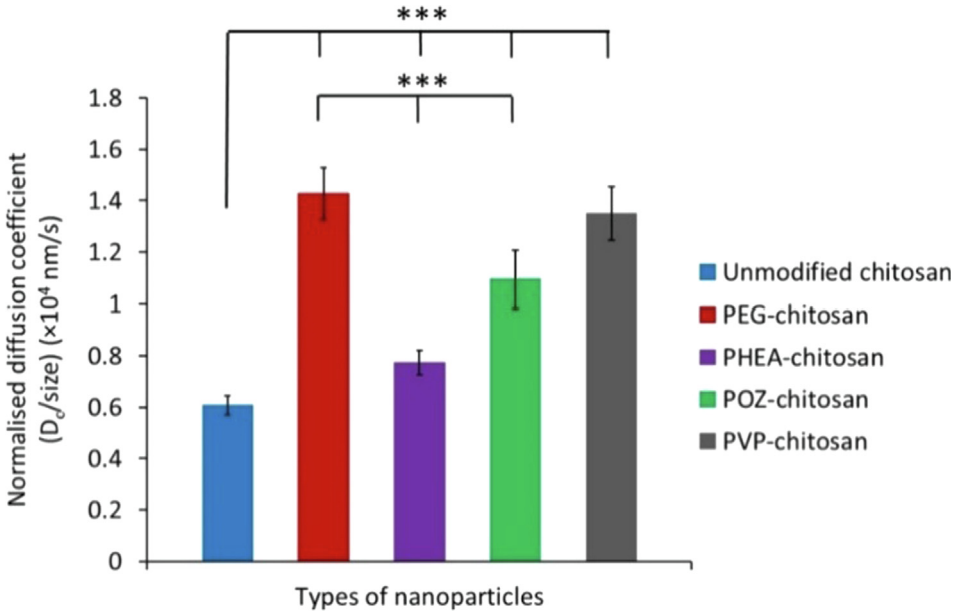

Fig. 5. Normalised experimentally determined diffusion coefficient of Alexa Fluor™ 546-labelled unmodified and modified chitosan-TPP nanoparticles through 0.5% w/v BSM solution. The diameter obtained from the DLS analysis was used to normalise the diffusion data. One-way ANOVA between chitosan and each of modified chitosan nanoparticles, and also between PEG- and each of PHEA-, POZ- and PVP-chitosan nanoparticles was performed; there is no significant difference ($p = 0.063$) between PEG- and PVP-chitosan nanoparticles, *** denotes $p < 0.001$ (mean ± SD, n = 9).

tion) and the negatively charged components of the gastrointestinal mucosa was expected. Zhang et al. [47] claimed that they were the first research group who reported the ability of PEGylated chitosan/DNA nanocomplexes to enhance the transport of DNA through artificial mucus using a Transwell mucus permeation assay. However, to our knowledge no studies on the diffusion of PEGylated chitosan-TPP nanoparticles in mucin solution using NTA have been reported.

The NTA data showed the following order of diffusivity in BSM solutions: PEG = PVP > POZ > PHEA > unmodified chitosan nanoparticles. This was evident from the higher normalised mean diffusion coefficient of the modified chitosan nanoparticles in 0.5% w/v BSM solution compared to unmodified chitosan nanoparticles (Fig. 5). In addition to the mean diffusion coefficient, the distribution of diffusion coefficient of the nanoparticles in 0.5% w/v BSM solution was determined, which also indicated higher diffusivity of the modified chitosan nanoparticles compared to the unmodified chitosan nanoparticles (Fig. 6).

It can, thus, be concluded that in all cases modification of chitosan with non-ionic polymers resulted in improved diffusivity of the nanoparticles in BSM. However, PEG and PVP showed better enhancement of diffusivity compared to POZ and PHEA.

Further studies on diffusion were performed using freshly excised sheep nasal mucosa. This sheep model was selected mainly due to its large nares and anatomical similarity of the nasal cavity with the human nose [61-64]. The nanoparticles showed different depths of penetration into sheep nasal mucosa (Fig. 7 and Fig. S25). After 5 and 15 min of incubation, all the nanoparticles based on modified chitosan penetrated significantly deeper into the nasal mucosa compared to unmodified chitosan ($p < 0.001$). However,

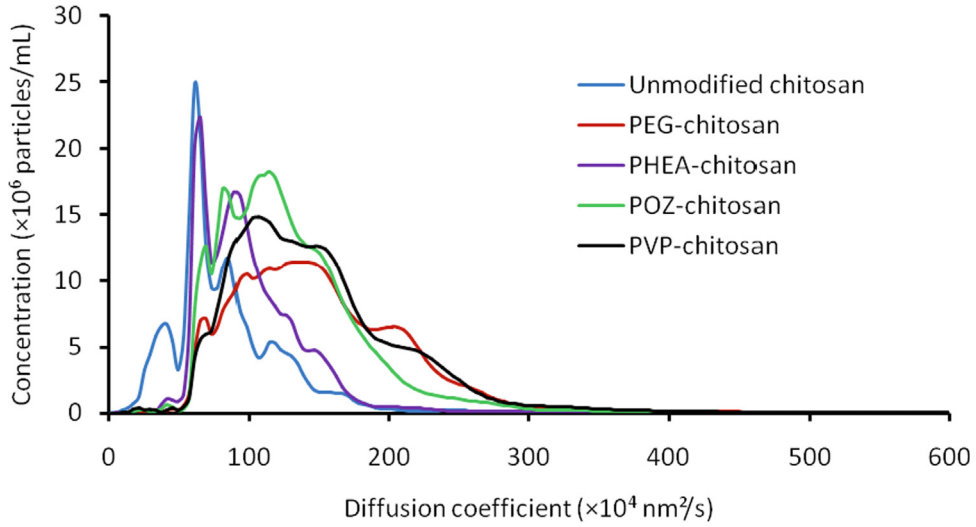

Fig. 6. Distribution of diffusion coefficient of Alexa Fluor™ 546-labelled unmodified and modified chitosan nanoparticles in 0.5% w/v BSM solution measured at 25 °C using NTA (mean, n = 9).

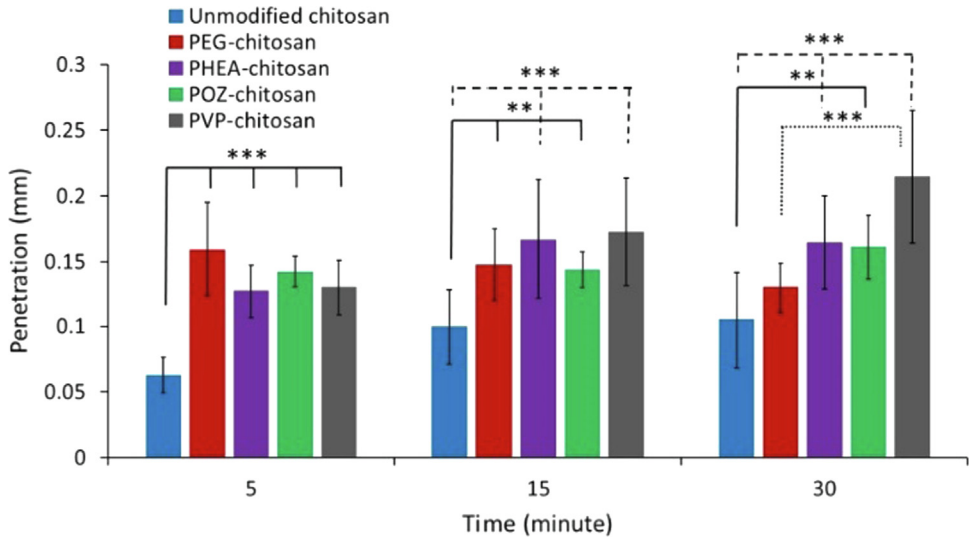

Fig. 7. Comparison of penetration depth of unmodified and modified chitosan nanoparticles into the freshly excised sheep nasal mucosa after 5, 15 and 30 min of incubation. Values represent the mean penetration across 10 separate tissue sections ± standard deviation.*** denotes $p < 0.001$, ** denotes $p < 0.01$.

at 30 min interval, there was no statistically significant difference ($p = 0.08$) between the penetration depth of unmodified chitosan nanoparticles and PEGylated chitosan nanoparticles. On the contrary, PHEA-, POZ- and PVP-chitosan nanoparticles showed a significantly greater penetration compared to unmodified chitosan at all time points. In fact, the modified chitosan nanoparticles were found to be in close proximity to the nasal epithelial cells (Fig. S26 and S27). It is clear that correlation exists between the diffusion coefficients of nanoparticles in BSM measured using NTA and the depth of nanoparticle penetration into sheep nasal mucosa. Modified chitosan nanoparticles showed a greater diffusivity than the unmodified chitosan nanoparticles. However, the difference in the barrier properties and the biochemical composition of the media in the NTA study (BSM solution) and *ex vivo* penetration study (sheep nasal mucosa) could explain the lack of difference between the penetration depth of unmodified chitosan and PEG-chitosan nanoparticles at the longer incubation time (30 min). The pH of the BSM solution used in our study was 5.5 but no literature has reported the pH of sheep nasal mucosa, nevertheless studies suggested the presence of acidic and neutral polysaccharides in the sheep nasal mucosa [65]. The pH of human nasal mucosa has been found to be in the range of 5.3–7.0 [66-69]. Additional factors that may play important roles in the barrier function of mucus is the presence of free thiol groups in fresh mucins compared to commercial BSM.

The mucus-penetrating properties of short-chain PEG coatings on nanoparticles are well-documented in the pharmaceutical literature [24,70,71]. Recently, we reported the possibility of using poly (2-methyl-2-oxazoline) and poly(2-ethyl-2-oxazoline) as new polymers with mucus-penetrating properties [30,31]. However, the demonstration of their enhanced mucus-penetration was done using model silica nanoparticles, not suitable for drug delivery because of their non-porous nature. In this study poly(2-ethyl-2-oxazoline) (POZ) was grafted to chitosan, a pharmaceutically relevant polymer and nanoparticles decorated with POZ also exhibited mucus-penetrating properties. To the best of our knowledge, this is also the first study reporting the use of short-chain PVP and PHEA for nanoparticle surface modification to enhance their mucus penetration. The nanoparticles prepared from chitosan modified with PVP exhibited the greatest diffusivity both in BSM solutions and also into sheep nasal mucosa compared to other non-ionic polymers used. Further optimisation of mucus-penetrating properties of the nanoparticles could be additionally achieved by varying the degrees of substitution of chitosan with non-ionic polymers.

4. Conclusions

We synthesised four derivatives of chitosan by reacting it with carboxyl-terminated PEG, PHEA, POZ and PVP. The modified chitosan showed complete solubility at any physiologically relevant pH (between 3 and 10) whereas unmodified chitosan precipitated at pH $\geq$ 7.3. This improvement in the solubility can dramatically broaden the range of applications of chitosan. Nanoparticles were prepared from unmodified and modified chitosan by complexation with tripolyphosphate. The modified chitosan nanoparticles showed an enhanced diffusivity in BSM solution compared to unmodified chitosan nanoparticles. They also penetrated deeper into sheep nasal mucosa compared to unmodified chitosan nanoparticles. The nanoparticles prepared from chitosan modified with PVP exhibited superior diffusivity compared to other non-ionic polymers used. As such, PVP has been identified as a novel mucus penetrating polymer. In the future, drug loaded nanoparticles could be prepared using these modified chitosans. It is expected that drug molecules could additionally affect the structure of the nanoparticles and their ability to penetrate the mucosa.

CRediT authorship contribution statement

Twana Mohammed M. Ways: Investigation, Methodology, Writing – original draft. **Sergey K. Filippov:** Investigation, Methodology, Funding acquisition, Writing – original draft, Writing – review & editing. **Samarendra Maji:** Investigation. **Mathias Glassner:** Investigation. **Michal Cegłowski:** Investigation. **Richard Hoogenboom:** Supervision, Writing – review & editing. **Stephen King:** Investigation, Writing – review & editing. **Wing Man Lau:** Supervision, Funding acquisition, Writing – review & editing. **Vitaliy V. Khutoryanskiy:** Conceptualization, Supervision, Funding acquisition, Writing – review & editing.

Declaration of Competing Interest

The authors declare the following financial interests/personal relationships which may be considered as potential competing interests: Twana Mohammed M. Ways reports financial support that was provided by HCED-Iraq and Ministry of Higher Education and Scientific Research-Kurdistan Regional Government. Vitaliy Khutoryanskiy reports financial support that was provided by the Leverhulme Trust.

Acknowledgements

We are thankful to HCED-Iraq and Ministry of Higher Education and Scientific Research-Kurdistan Regional Government for their support. SKF and VVK are also grateful to the Leverhulme Trust for the visiting professorship grant (VP2-2020-013). Additionally, we are grateful to STFC for providing access to SANS beam time (proposal RB1810863). We acknowledge the assistance of staff at the Chemical Analysis Facility (CAF, University of Reading) in NMR, FTIR, fluorescence spectroscopy and TEM experiments.

Appendix A. Supplementary material

^{1}H-NMR and FTIR spectra of unmodified and modified chitosan, washing after dialysis of the Alexa Fluor™ 546-labelled chitosan, fluorescence calibration curve, optimisation of unmodified chitosan-TPP nanoparticles, SANS curves of chitosan nanoparticles, temperature versus viscosity profile of 0.5% w/v BSM solution and exemplar fluorescent images showing penetration of Alexa Fluor™ 546-labelled unmodified and modified chitosan nanoparticles

Supplementary data to this article can be found online at https://doi.org/10.1016/j.jcis.2022.06.126.

References

[1] N.A. Peppas, J.J. Sahlin, Hydrogels as mucoadhesive and bioadhesive materials: A review, Biomaterials 17 (16) (1996) 1553–1561.
[2] H. Batchelor, Bioadhesive dosage forms for esophageal drug delivery, Pharm. Res.-Dordr. 22 (2) (2005) 175–181.
[3] A. Ludwig, The use of mucoadhesive polymers in ocular drug delivery, Adv. Drug Deliver Rev. 57 (11) (2005) 1595–1639.
[4] M.I. Ugwoke, R.U. Agu, N. Verbeke, R. Kinget, Nasal mucoadhesive drug delivery: Background, applications, trends and future perspectives, Adv. Drug Deliver. Rev. 57 (11) (2005) 1640–1665.
[5] A. Sosnik, J. das Neves, B. Sarmento, Mucoadhesive polymers in the design of nano-drug delivery systems for administration by non-parenteral routes: A review, Prog. Polym. Sci. 39(12) (2014) 2030-2075.
[6] V.V. Khutoryanskiy, Mucoadhesive materials and drug delivery systems, John Wiley & Sons Inc, Chichester, West Sussex, 2014.
[7] C.M. Caramella, S. Rossi, F. Ferrari, M.C. Bonferoni, G. Sandri, Mucoadhesive and thermogelling systems for vaginal drug delivery, Adv. Drug Deliver. Rev. 92 (2015) 39–52.
[8] O.M. Kolawole, W.M. Lau, H. Mostafid, V.V. Khutoryanskiy, Advances in intravesical drug delivery systems to treat bladder cancer, Int. J. Pharmaceut. 532 (1) (2017) 105–117.
[9] A.R. Khan, M.R. Liu, M.W. Khan, G.X. Zhai, Progress in brain targeting drug delivery system by nasal route, J. Control. Release 268 (2017) 364–389.

[10] C.M. Lehr, F.G.J. Poelma, H.E. Junginger, J.J. Tukker, An Estimate of Turnover Time of Intestinal Mucus Gel Layer in the Rat Insitu Loop, Int. J. Pharmaceut. 70 (3) (1991) 235–240.
[11] L. Illum, Nasal drug delivery—possibilities, problems and solutions, J. Control. Release 87 (1) (2003) 187–198.
[12] J.R. Harkema, S.A. Carey, J.G. Wagner, The nose revisited: A brief review of the comparative structure, function, and toxicologic pathology of the nasal epithelium, Toxicol. Pathol. 34 (3) (2006) 252–269.
[13] H.H. Sigurdsson, J. Kirch, C.M. Lehr, Mucus as a barrier to lipophilic drugs, Int. J. Pharmaceut. 453 (1) (2013) 56–64.
[14] L.M. Ensign, R. Cone, J. Hanes, Oral drug delivery with polymeric nanoparticles: The gastrointestinal mucus barriers, Adv. Drug Deliver Rev. 64 (6) (2012) 557–570.
[15] P.G. Bhat, D.R. Flanagan, M.D. Donovan, Drug diffusion through cystic fibrotic mucus: Steady-state permeation, rheologic properties, and glycoprotein morphology, J. Pharm. Sci. 85 (6) (1996) 624–630.
[16] N.N. Sanders, S.C. De Smedt, E. Van Rompaey, P. Simoens, F. De Baets, J. Demeester, Cystic fibrosis sputum: a barrier to the transport of nanospheres, Am. J. Respir. Crit. Care Med. 162 (5) (2000) 1905–1911.
[17] S. Azarmi, W.H. Roa, R. Loebenberg, Targeted delivery of nanoparticles for the treatment of lung diseases, Adv. Drug Deliver Rev. 60 (8) (2008) 863–875.
[18] D.A. Edwards, A. Ben-Jebria, R. Langer, Recent advances in pulmonary drug delivery using large, porous inhaled particles, J. Appl. Physiol. 85 (2) (1998) 379–385.
[19] J. das Neves, M. Amiji, B. Sarmento, Mucoadhesive nanosystems for vaginal microbicide development: friend or foe?, Wiley Interdiscip Rev. Nanomed. Nanobiotechnol. 3(4) (2011) 389-99.
[20] D. Lopes, C. Nunes, M.C.L. Martins, B. Sarmento, S. Reis, Eradication of Helicobacter pylori: Past, present and future, J. Control. Release 189 (2014) 169–186.
[21] J. Xu, J.J. Heys, V.H. Barocas, T.W. Randolph, Permeability and diffusion in vitreous humor: Implications for drug delivery, Pharm. Res.-Dordr 17 (6) (2000) 664–669.
[22] Q. Xu, N.J. Boylan, J.S. Suk, Y.Y. Wang, E.A. Nance, J.C. Yang, P.J. McDonnell, R.A. Cone, E.J. Duh, J. Hanes, Nanoparticle diffusion in, and microrheology of, the bovine vitreous ex vivo, J. Control. Release 167 (1) (2013) 76–84.
[23] Y.Y. Wang, S.K. Lai, J.S. Suk, A. Pace, R. Cone, J. Hanes, Addressing the PEG Mucoadhesivity Paradox to Engineer Nanoparticles that "Slip" through the Human Mucus Barrier, Angew Chem. Int. Edit. 47 (50) (2008) 9726–9729.
[24] S.K. Lai, D.E. O'Hanlon, S. Harrold, S.T. Man, Y.Y. Wang, R. Cone, J. Hanes, Rapid transport of large polymeric nanoparticles in fresh undiluted human mucus, Proc. Natl. Acad. Sci. USA 104 (5) (2007) 1482–1487.
[25] G. Costabile, R. Provenzano, A. Azzalin, V.C. Scoffone, L.R. Chiarelli, V. Rondelli, I. Grillo, T. Zinn, A. Lepioshkin, S. Savina, A. Miro, F. Quaglia, V. Makarov, T. Coenye, P. Brocca, G. Riccardi, S. Buroni, F. Ungaro, PEGylated mucus-penetrating nanocrystals for lung delivery of a new FtsZ inhibitor against Burkholderia cenocepacia infection, Nanomed.: Nanotechnol. Biol. Med. 23 (2020) 102113.
[26] H. Sato, Y. Kaneko, K. Yamada, K.D. Ristroph, H.D. Lu, Y. Seto, H.-K. Chan, R.K. Prud'homme, S. Onoue, Polymeric Nanocarriers With Mucus-Diffusive and Mucus-Adhesive Properties to Control Pharmacokinetic Behavior of Orally Dosed Cyclosporine A, J. Pharm. Sci. 109(2) (2020) 1079-1085.
[27] R. Nunes, F. Araújo, J. Tavares, B. Sarmento, J. das Neves, Surface modification with polyethylene glycol enhances colorectal distribution and retention of nanoparticles, Eur. J. Pharm. Biopharm. 130 (2018) 200-206.
[28] R. Machado Cruz, M.J. Santos-Martinez, L. Tajber, Impact of polyethylene glycol polymers on the physicochemical properties and mucoadhesivity of itraconazole nanoparticles, Eur. J. Pharm. Biopharm. 144 (2019) 57–67.
[29] V.V. Khutoryanskiy, Beyond PEGylation: Alternative surface-modification of nanoparticles with mucus-inert biomaterials, Adv Drug Deliver Rev 124 (2018) 140–149.
[30] E.D.H. Mansfield, V.R. de la Rosa, R.M. Kowalczyk, I. Grillo, R. Hoogenboom, K. Sillence, P. Hole, A.C. Williams, V.V. Khutoryanskiy, Side chain variations radically alter the diffusion of poly(2-alkyl-2-oxazoline) functionalised nanoparticles through a mucosal barrier, Biomater. Sci. 4 (9) (2016) 1318–1327.
[31] E.D. Mansfield, K. Sillence, P. Hole, A.C. Williams, V.V. Khutoryanskiy, POZylation: a new approach to enhance nanoparticle diffusion through mucosal barriers, Nanoscale 7 (32) (2015) 13671–13679.
[32] C.J. Ferguson, R.J. Hughes, D. Nguyen, B.T.T. Pham, R.G. Gilbert, A.K. Serelis, C.H. Such, B.S. Hawkett, Ab initio emulsion polymerization by RAFT-controlled self-assembly, Macromolecules 38 (6) (2005) 2191–2204.
[33] G. Pound, Z. Eksteen, R. Pfukwa, J.M. McKenzie, R.F.M. Lange, B. Klumperman, Unexpected reactions associated with the xanthate-mediated polymerization of N-vinylpyrrolidone, J. Polym. Sci., Part A: Polym. Chem. 46 (19) (2008) 6575–6593.
[34] N. Bhattarai, H.R. Ramay, J. Gunn, F.A. Matsen, M. Zhang, PEG-grafted chitosan as an injectable thermosensitive hydrogel for sustained protein release, J. Control. Release 103 (3) (2005) 609–624.
[35] I.A. Sogias, A.C. Williams, V.V. Khutoryanskiy, Why is chitosan mucoadhesive?, Biomacromolecules 9 (2008) 1837–1842
[36] P. Calvo, C. Remuñán-López, J.L. Vila-Jato, M.J. Alonso, Novel hydrophilic chitosan-polyethylene oxide nanoparticles as protein carriers, J. Appl. Polym. Sci. 63 (1) (1997) 125–132.
[37] https://www.mantidproject.org.
[38] G.D. Wignall, F.S. Bates, Absolute calibration of small-angle neutron scattering data, J. Appl. Crystallogr. 20 (1) (1987) 28–40.
[39] B. Hammouda, Small-Angle Scattering From Branched Polymers, Macromol. Theory Simul. 21 (6) (2012) 372–381.
[40] T.M.M. Ways, W.M. Lau, V.V. Khutoryanskiy, Chitosan and its derivatives for application in mucoadhesive drug delivery systems, Polymers 10 (3) (2018) 267.
[41] J. Wu, X. Wang, J.K. Keum, H. Zhou, M. Gelfer, C.A. Avila-Orta, H. Pan, W. Chen, S.M. Chiao, B.S. Hsiao, B. Chu, Water soluble complexes of chitosan-g-MPEG and hyaluronic acid, J Biomed Mater Res A 80 (4) (2007) 800–812.
[42] Q. Luo, H. Gao, L. Peng, G. Liu, Z. Zhang, Synthesis of PEGylated chitosan copolymers as efficiently antimicrobial coatings for leather, J. Appl. Polym. Sci. 133 (22) (2016) 43465–43472.
[43] L. Casettari, D. Vllasaliu, G. Mantovani, S.M. Howdle, S. Stolnik, L. Illum, Effect of PEGylation on the toxicity and permeability enhancement of chitosan, Biomacromolecules 11 (2010) 2854–2865.
[44] Q.Z. Wang, X.G. Chen, N. Liu, S.X. Wang, C.S. Liu, X.H. Meng, C.G. Liu, Protonation constants of chitosan with different molecular weight and degree of deacetylation, Carbohydr. Polym. 65 (2) (2006) 194–201.
[45] M. Rinaudo, Chitin and chitosan: Properties and applications, Prog. Polym. Sci. 31 (7) (2006) 603–632.
[46] I.A. Sogias, V.V. Khutoryanskiy, A.C. Williams, Exploring the factors affecting the solubility of chitosan in water, Macromol. Chem. Phys. 211 (4) (2010) 426–433.
[47] H. Zhang, T.F. Bahamondez-Canas, Y. Zhang, J. Leal, H.D.C. Smyth, Pegylated chitosan for nonviral aerosol and mucosal delivery of the CRISPR/Cas9 system *in vitro*, Mol. Pharm. 15 (11) (2018) 4814–4826.
[48] A. Murmiliuk, S.K. Filippov, O. Rud, P. Košovan, Z. Tošner, A. Radulescu, A. Skandalis, S. Pispas, M. Šlouf, M. Štěpánek, Reversible multilayered vesicle-like structures with fluid hydrophobic and interpolyelectrolyte layers, J. Colloid Interface Sci. 599 (2021) 313–325.
[49] D. Geißler, C. Gollwitzer, A. Sikora, C. Minelli, M. Krumrey, U. Resch-Genger, Effect of fluorescent staining on size measurements of polymeric nanoparticles using DLS and SAXS, Anal. Methods 7 (23) (2015) 9785–9790.
[50] E.D.H. Mansfield, Y. Pandya, E.A. Mun, S.E. Rogers, I. Abutbul-Ionita, D. Danino, A.C. Williams, V.V. Khutoryanskiy, Structure and characterisation of hydroxyethylcellulose–silica nanoparticles, RSC Adv. 8 (12) (2018) 6471–6478.
[51] V. Filipe, A. Hawe, W. Jiskoot, Critical evaluation of nanoparticle tracking analysis (NTA) by nanosight for the measurement of nanoparticles and protein aggregates, Pharm. Res. 27 (5) (2010) 796–810.
[52] J. Gross, S. Sayle, A.R. Karow, U. Bakowsky, P. Garidel, Nanoparticle tracking analysis of particle size and concentration detection in suspensions of polymer and protein samples: Influence of experimental and data evaluation parameters, Eur. J. Pharm. Biopharm. 104 (2016) 30–41.
[53] E.A. Mun, C. Hannell, S.E. Rogers, P. Hole, A.C. Williams, V.V. Khutoryanskiy, On the role of specific interactions in the diffusion of nanoparticles in aqueous polymer solutions, Langmuir 30 (1) (2014) 308–317.
[54] L. Achar, N.A. Peppas, Preparation, characterisation and mucoadhesive interactions of poly (methacrylic acid) copolymers with rat mucosa, J. Control. Release 31 (1994) 271–276.
[55] A. Mistry, S. Stolnik, L. Illum, Nanoparticles for direct nose-to-brain delivery of drugs, Int. J. Pharm. 379 (1) (2009) 146–157.
[56] Y.A. Albarkah, R.J. Green, V.V. Khutoryanskiy, Probing the mucoadhesive interactions between porcine gastric mucin and some water-soluble polymers, Macromol. Biosci. 15 (11) (2015) 1546–1553.
[57] N.A. Fefelova, Z.S. Nurkeeva, G.A. Mun, V.V. Khutoryanskiy, Mucoadhesive interactions of amphiphilic cationic copolymers based on [2-(methacryloyloxy)ethyl]trimethylammonium chloride, Int. J. Pharm. 339 (1) (2007) 25–32.
[58] L.H. Chuah, C.J. Roberts, N. Billa, S. Abdullah, R. Rosli, S. Manickam, Using nanoparticle tracking analysis (NTA) to decipher mucoadhesion propensity of curcumin-containing chitosan nanoparticles and curcumin release, J. Dispersion Sci. Technol. 35 (9) (2014) 1201–1207.
[59] T.M.M. Ways, W.M. Lau, K.W. Ng, V.V. Khutoryanskiy, Synthesis of thiolated, PEGylated and POZylated silica nanoparticles and evaluation of their retention on rat intestinal mucosa *in vitro*, Eur. J. Pharm. Sci. 122 (2018) 230–238.
[60] C. Prego, D. Torres, E. Fernandez-Megia, R. Novoa-Carballal, E. Quinoa, M.J. Alonso, Chitosan-PEG nanocapsules as new carriers for oral peptide delivery: Effect of chitosan pegylation degree, J. Control. Release 111 (3) (2006) 299–308.
[61] C. Tas, C.K. Ozkan, A. Savaser, Y. Ozkan, U. Tasdemir, H. Altunay, Nasal administration of metoclopramide from different dosage forms: *In vitro*, *ex vivo*, and *in vivo* evaluation, Drug Deliv. 16 (3) (2009) 167–175.
[62] L. Macias-Valle, A. Finkelstein-Kulka, J. Manji, C. Okpaleke, S. Al-Salihi, A.R. Javer, Evaluation of sheep sinonasal endoscopic anatomy as a model for rhinologic research, World Journal of Otorhinolaryngology -, Head and Neck Surgery (2018).
[63] A.W. Barrios, P. Sanchez Quinteiro, I. Salazar, The nasal cavity of the sheep and its olfactory sensory epithelium, Microsc Res Tech 77 (12) (2014) 1052–1059.
[64] L. Illum, Nasal delivery. The use of animal models to predict performance in man, J. Drug Target. 3 (6) (1996) 427–442.

[65] D. Ibrahim, N. Nakamuta, K. Taniguchi, Y. Yamamoto, K. Taniguchi, Histological and lectin histochemical studies on the olfactory and respiratory mucosae of the sheep, J. Vet. Med. Sci. 76 (3) (2014) 339–346.
[66] N.J. Ireson, J.S. Tait, G.A. MacGregor, E.H. Baker, Comparison of nasal pH values in black and white individuals with normal and high blood pressure, Clin. Sci. 100 (2001) 327–333.
[67] R.J.A. England, J.J. Homer, L.C. Knight, S.R. Ell, Nasal pH measurement: A reliable and repeatable parameter, Clin. Otolaryngol. 24 (1999) 67–68.
[68] B.A. Aderibigbe, In situ-based gels for nose to brain delivery for the treatment of neurological diseases, Pharmaceutics 10 (2) (2018) 40.
[69] S.K. Lai, J.S. Suk, A. Pace, Y.-Y. Wang, M. Yang, O. Mert, J. Chen, J. Kim, J. Hanes, Drug carrier nanoparticles that penetrate human chronic rhinosinusitis mucus, Biomaterials 32 (26) (2011) 6285–6290.
[70] Y.-Y. Wang, S.K. Lai, J.S. Suk, A. Pace, R. Cone, J. Hanes, Addressing the PEG Mucoadhesivity Paradox to Engineer Nanoparticles that "Slip" through the Human Mucus Barrier, Angew. Chem. Int. Ed. 47 (50) (2008) 9726–9729.
[71] M. Yang, S.K. Lai, Y.-Y. Wang, W. Zhong, C. Happe, M. Zhang, J. Fu, J. Hanes, Biodegradable Nanoparticles Composed Entirely of Safe Materials that Rapidly Penetrate Human Mucus, Angew. Chem. Int. Ed. 50 (11) (2011) 2597–2600.